Hypersonic Mach Number and Real Gas Effects on Space Shuttle Orbiter Aerodynamics

J.R. Maus,* B.J. Griffith,† and K.Y. Szema‡
Calspan Field Services, Inc., Arnold Air Force Station, Tennessee
and
J.T. Best§
Arnold Engineering Development Center, Arnold Air Force Station, Tennessee

Inviscid computational fluid dynamics (CFD) codes, verified by ground test data, have been applied to a modified Space Shuttle Orbiter geometry to investigate differences between preflight aerodynamic predictions and aerodynamic data from hypersonic re-entry flight. Results of the study indicate that the differences between flight and pre-STS-1 predictions of hypersonic pitching moment are primarily due to Mach number and real gas effects.

Nomenclature

A	= reference area, 2690 ft^2
C_A	= axial force coefficient, F_A/Aq_∞
C_m	= pitching moment coefficient, m_0/cAq_∞
C_N	= normal force coefficient, F_N/Aq_∞
C_p	= pressure coefficient, $(p\text{-}p_\infty)/q_\infty$
c	= reference length, 474.72 in.
D	= drag force
F	= force component
L	= lift force or body length
M	= Mach number
m_0	= total moment about $x_0 = 840.7$ in., $z_0 = 37.0$ in.
p	= pressure
q	= dynamic pressure
$Re_{\infty L}$	= freestream Reynolds number based on model length
V	= velocity
x,y,z	= Cartesian coordinates
α	= angle of attack
γ	= specific heat ratio
δ	= deflection angle

Subscripts

bf	= body flap
c	= centroid
cp	= center of pressure
e	= elevon
∞	= freestream conditions

Introduction

ALTHOUGH the flight test program for the Space Shuttle has been remarkably successful overall, a number of aerodynamic anomalies has arisen that requires further investigation. For example, results from the first three Space Shuttle flights have shown a significant difference between preflight prediction of hypersonic pitching moment and values inferred from flight data.[1,2] These differences have resulted in body flap deflections, required to maintain trim, greater than indicated by preflight predictions.

The preflight predictions of the Orbiter aerodynamics were based primarily on ground test data obtained in a very extensive wind tunnel test program. In an effort to resolve this discrepancy, the present study addresses, through the use of computational fluid dynamics (CFD) codes, some of the fundamental flow modeling necessary to extrapolate ground test data to hypersonic flight conditions. In particular, this paper examines the high Mach number and real gas effects on the Orbiter aerodynamics. The effects of Mach number were assesed by parametrically varying freestream Mach number and angle of attack in a series of perfect gas computations. Real gas effects were explored by making calculations at specific points of the re-entry trajectory using equilibrium air thermodynamics and comparing these calculations with the corresponding perfect gas computations.

Approach

Advanced CFD codes CM3DT[3] and STEIN[4] have been applied to a modified Orbiter geometry to obtain detailed inviscid flowfield solutions for both wind tunnel test conditions and hypersonic flight conditions. CM3DT is a transonic blunt-body code that was used to provide a starting solution for the supersonic afterbody code, STEIN. Figure 1 illustrates the geometry for which the computations were performed. The major differences between the computational model geometry and the actual Orbiter geometry, shown in Fig. 2, are as follows: 1) the wing sweep-back angle has been increased from 45 to 55 deg; 2) the wing thickness of the model is about twice that of the Orbiter; 3) the computational geometry is squared off at the body flap hinge line; and 4) the rudder and OMS pods are not included in the model geometry. These modifications to the geometry were designed to avoid embedded subsonic flow regions at the wing-body junction and complex leeside flow features that have little influence on the aerodynamics at high angles of attack. The computational geometry was obtained from NASA/LaRC and was not altered during the course of this investigation. The projected planform area of the computational geometry is about 2% less than the Orbiter projected area, and the centroid of the computational projected area is approximately 2% of model length further aft than that of the Orbiter.

CM3DT and STEIN are both interfaced with the QUICK[5] geometry routines which specify the body shape and compute

Presented as Paper 83-0343 at the AIAA 21st Aerospace Sciences Meeting, Reno, Nev., Jan. 10-13, 1983; submitted Feb. 3, 1983; revision received July 11, 1983

*Research Engineer, Aerodynamics Projects Branch, AEDC Division. Member AIAA.
†Section Supervisor, Aerodynamics Projects Branch, AEDC Division. Associate Fellow AIAA.
‡Research Engineer, AEDC Division; now Research Engineer with Rockwell International Science Center, Thousands Oaks, Calif. Member AIAA.
§Project Manager, U.S. Air Force. Member AIAA.

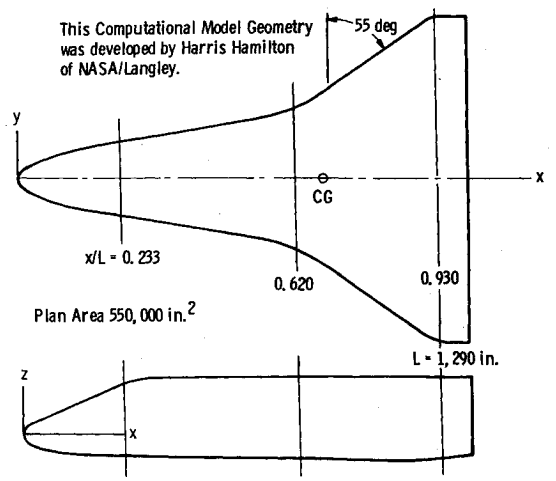

Fig. 1a Computational model geometry, plan and elevation views.

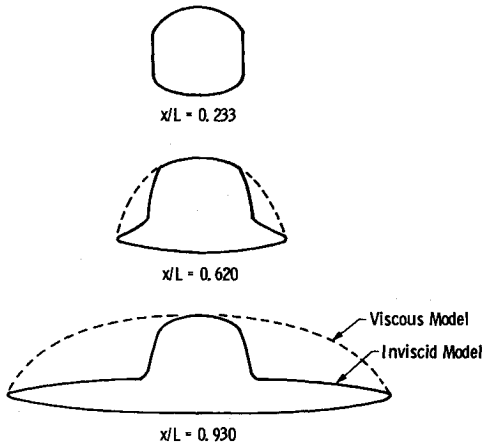

Fig. 1b Computational model geometry, cross sections.

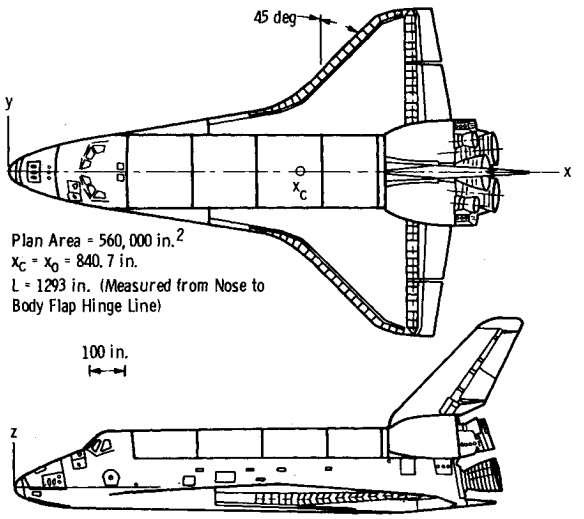

Fig. 2 Shuttle Orbiter geometry.

geometrical parameters on the surface. Both codes employ conformal mapping to transform physical space between the body and the bow shock into a simple computational domain. Calculated surface pressures were integrated over the body to obtain aerodynamic forces and moments acting on the vehicle.

Comparison with Wind Tunnel Data

To establish credibility of the CFD results and to assess the effect of geometrical differences on the aerodynamic

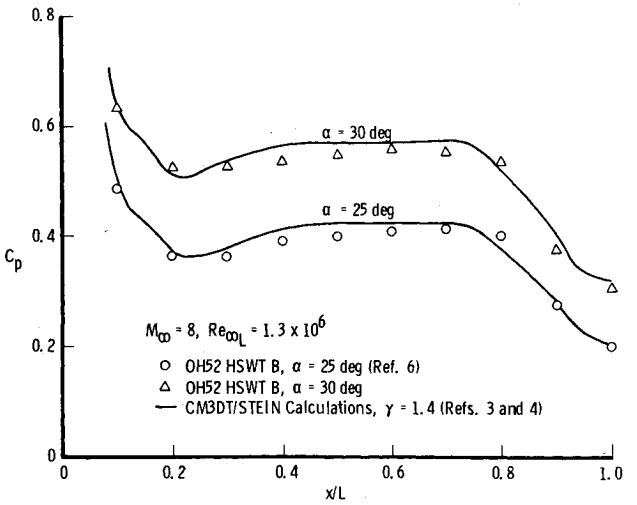

Fig. 3 Comparison of pressure distributions on windward centerline with experimental data.

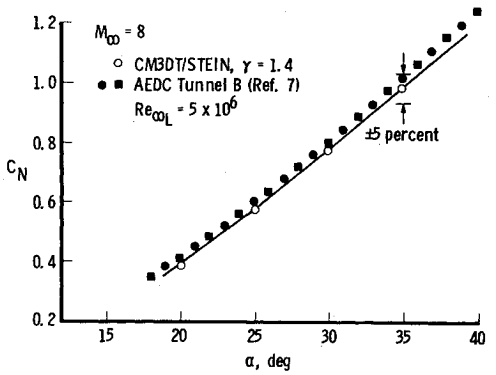

Fig. 4 Comparison of computed normal force coefficient with experimental data.

parameters, initial computations with CM3DT and STEIN were made to compare with wind tunnel results. The specific wind tunnel data used in this comparison are from AEDC Tunnel B.[6,7]

Figure 3 shows a comparison of computed and measured pressure coefficients along the windward centerline at $M_\infty = 8$ for two angles of attack. The computed pressure distribution, although slightly overpredicting the pressures in the midbody region, generally agrees very well in distribution and level with the experimental values.

A comparison of computed and experimental normal force coefficients is shown in Fig. 4. The reference area used to nondimensionalize the calculated values is the actual Orbiter wing area, $A = 2690$ ft^2.

Predicting pitching moment is a severe test of any CFD code. Figure 5 shows a comparison of computed pitching moment coefficient with experimental values for the basic Orbiter geometry. The maximum deviation, which occurs at an angle of attack of about 30 deg, corresponds to a difference in center of pressure of about 0.3% of the body length.

The results of the above comparisons, in addition to giving confidence in the applicability of the computational code to the complex model Orbiter geometry, also indicate that there are no great *aerodynamic* differences between the computational geometry and the actual Orbiter geometry for these high Mach number and high angle-of-attack test conditions.

Mach Number and Real Gas Effects

Effects on the Orbiter aerodynamics due to hypersonic Mach number and equilibrium air thermodynamics were

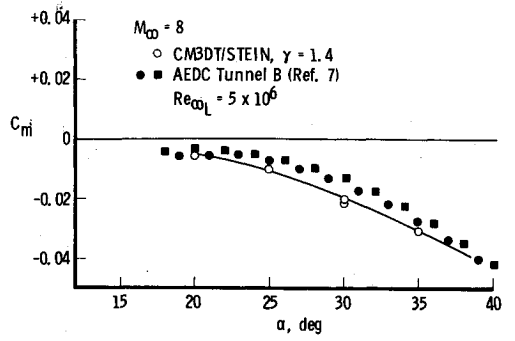

Fig. 5 Comparison of computed pitching moment coefficient with experimental data.

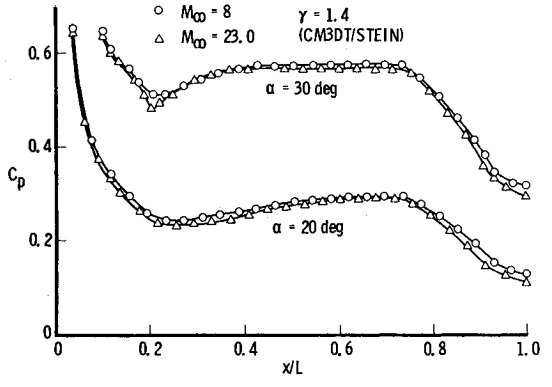

Fig. 6 Effect of Mach number on windward centerline pressure distributions.

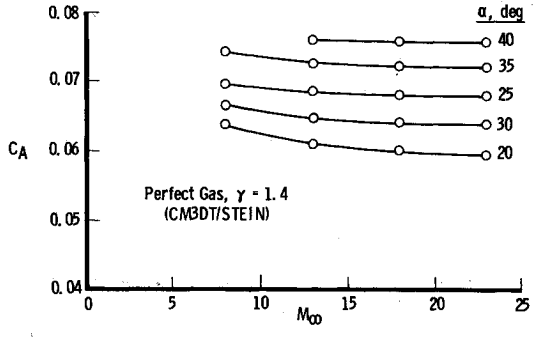

Fig. 7 Effect of Mach number on axial force coefficient.

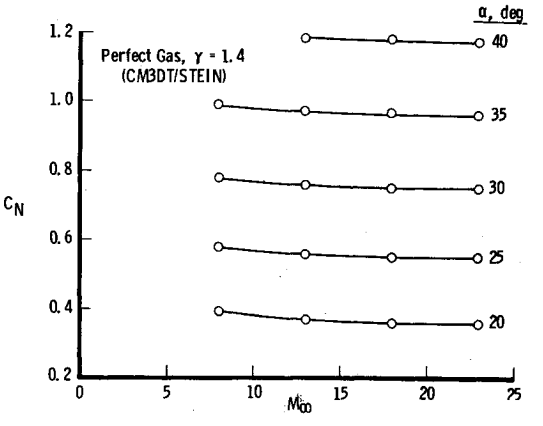

Fig. 8 Effect of Mach number on normal force coefficient.

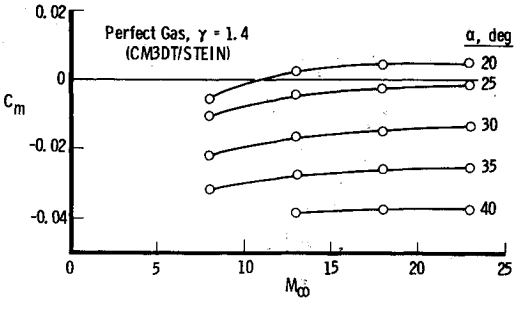

Fig. 9 Effect of Mach number on pitching moment coefficient.

Table 1 Matrix of conditions

α, deg	Gas	Mach number 8	13	18	23
20	Ideal	V[a]	V	V	V
	Real				V
25	Ideal	V	V	V	V
	Real				V
30	Ideal	V	V	V	V
	Real	V	V	V	V
35	Ideal	V	V	V	V
	Real	V	V	V	V
40	Ideal	X[b]	V	V	V
	Real		X	X	X

Real-gas conditions

M_∞	V_∞	Altitude, kft
8	8,600	152
13	14,000	188
18	18,000	212
23	22,000	240

[a] V = computation completed. [b] × = computation failed.

investigated by carrying out a series of CFD solutions using CM3DT and STEIN for the matrix of conditions shown in Table 1. As indicated in this table, difficulties were encountered in obtaining solutions at the highest angle of attack, $\alpha = 40$ deg.

Mach Number Effects

Figure 6 shows comparative pressure coefficient distributions along the windward centerline of the model Orbiter geometry for two angles of attack and Mach numbers of 8.0 and 23.0. The results in this figure were obtained assuming flow of an ideal gas with $\gamma = 1.4$. This figure reveals that increasing the Mach number causes a slight decrease in pressure coefficient along the centerline over the entire body; this decrease being somewhat greater on the aft portion of the vehicle.

The effect of Mach number variations on the aerodynamic coefficients C_A, C_N, and C_M are illustrated in Figs. 7, 8, and 9, respectively. Both the axial and normal force coefficients show a decrease with increasing Mach number due to the decreased pressure coefficients. The pitching moment coefficient increases (more nose up) with Mach number due to the decrease of pressure coefficient in the aft portion of the vehicle where the planform area is concentrated. The increase in pitching moment is most pronounced at low angles of attack. As expected, all three coefficients asymptotically approach constant values as the Mach number becomes large.

Figure 10 shows the forward shift in center of pressure from the reference condition at $M_\infty = 8$ as a function of Mach number and angle of attack. This figure indicates that for $M_\infty = 23$ the shift in center of pressure is approximately 11 in., forward for $\alpha = 20$ deg and 2½ in. forward for $\alpha = 35$ deg.

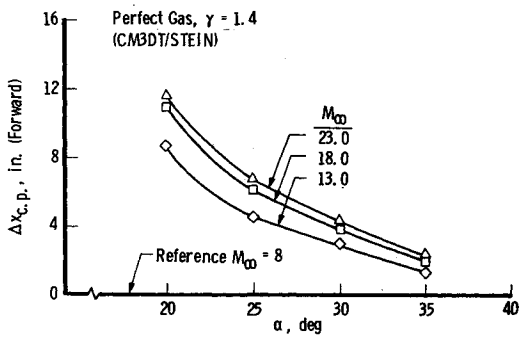

Fig. 10 Effect of Mach number on center of pressure location.

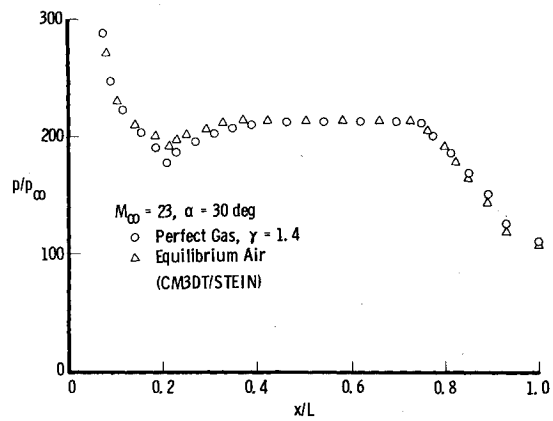

Fig. 11 Real gas effect on windward centerline pressure distribution.

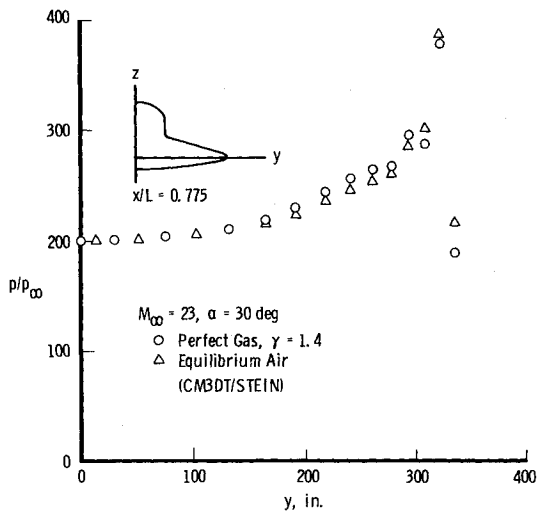

Fig. 12 Real gas effect on aft windward pressure distribution.

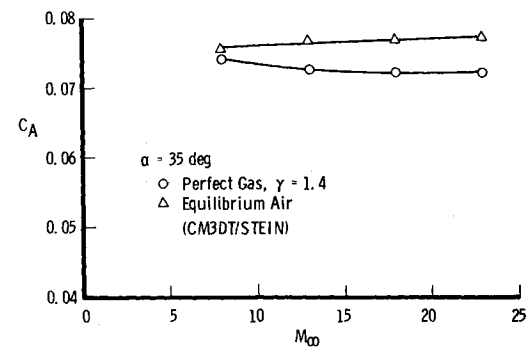

Fig. 13 Real gas effect on axial force coefficient.

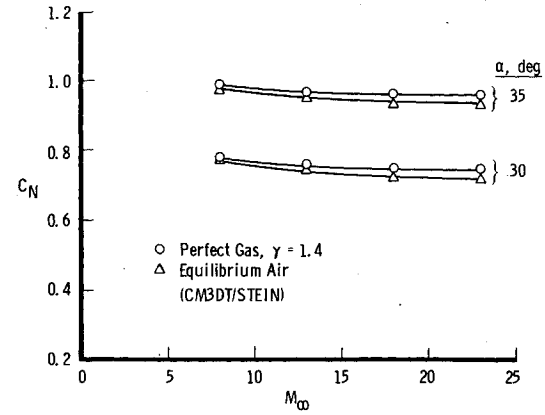

Fig. 14 Real gas effect on normal force coefficient.

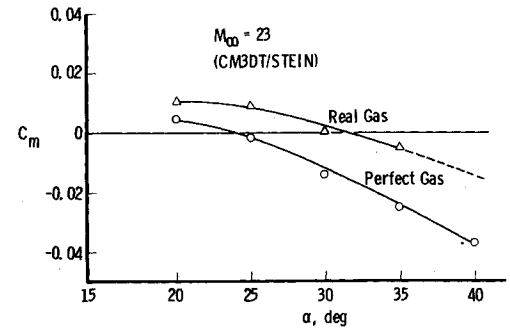

Fig. 15 Real gas effect on pitching moment coefficient.

Real Gas Effects

The effect of real gas thermodynamics on the surface pressure distribution is illustrated in Figs. 11 and 12 by comparing the pressure distribution for a perfect gas at $M_\infty = 23$ with an equilibrium air calculation for conditions at a point on the re-entry trajectory corresponding approximately to the same Mach number. Figure 11 shows comparative pressures along the windward centerline. Note that the real gas pressures are slightly higher than the perfect gas pressures in the forebody region and somewhat lower on the afterbody. These distributions indicate that an effect of real gas will be to produce a more positive (nose-up) pitching moment. Figure 12 displays comparative spanwise pressure distributions at $x/L = 0.775$ and shows that the real gas effects cause a reduced pressure over most of the aft windward portion of the body but an increase near the wing leading edge.

Real gas effects on the axial and normal force coefficients of the Shuttle Orbiter model are illustrated in Figs. 13 and 14. The Mach numbers for the real gas computations in these figures correspond to points of the re-entry trajectory given in Table 1. Figure 13 demonstrates that real gas effects increase the axial force coefficient with the increase being most pronounced for the high-velocity, high-altitude conditions. This increase is caused by higher pressures on the vehicle forebody and wing leading edge as shown in Figs. 11 and 12. Figure 14 indicates a slight decrease in normal force coefficient due to real gas effects caused by the lower pressures on the aft part of the Orbiter.

Real gas effects on pitching moment are illustrated for the high-velocity, high-altitude case in Fig. 15 by comparing the results for perfect gas computations with those for equilibrium air thermodynamics. This figure reveals that the real gas effects tend to drive C_m more positive with the effect being most significant at higher angles of attack.

The combined Mach number and real gas effects are illustrated in Fig. 16, for the high Mach number condition, in

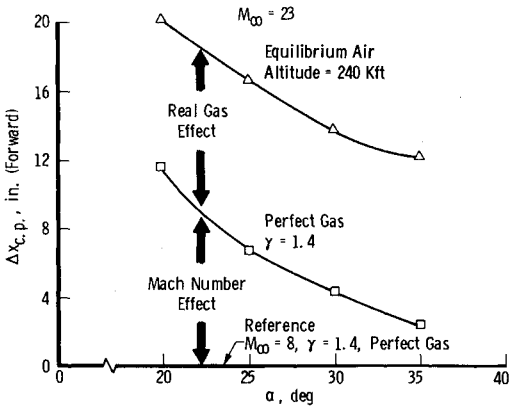

Fig. 16 Combined Mach number and real gas effects on center of pressure location.

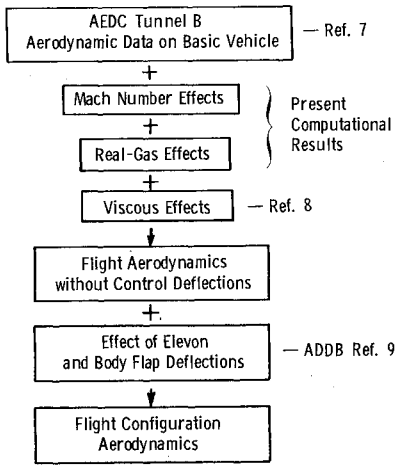

Fig. 17 Methodology for extrapolation to flight conditions.

terms of forward shift of the aerodynamic center of pressure from the baseline, $M_\infty = 8$, perfect gas case. This figure indicates that the shift in center of pressure is about 12 in. forward for an angle of attack of 35 deg and about 21 in. forward for an angle of attack of 20 deg, resulting in significant changes in the aerodynamics of the Shuttle.

Comparison with Flight Data

In order to make comparisons with flight results, aerodynamic coefficients for the Shuttle Orbiter under flight conditions were obtained by extrapolating wind tunnel data for $M_\infty = 8$.[7] The methodology that was employed in this extrapolation is illustrated in Fig. 17. The Mach number and real gas effects were obtained from the computational results described in the previous section. The viscous effects indicated in Fig. 17 were derived from a combination of computational results using a parabolized Navier-Stokes code and analysis of wind tunnel data. This work is described in detail in Ref. 8.

For the comparisons made in this paper, the contributions of the control surface deflections were assumed to be as predicted prior to flight.[9] In other words, it was assumed that the control surface effectiveness was not degraded by viscous effects nor substantially changed by Mach number and real gas effects.

An example of the buildup of flight C_m for the basic body is given in Fig. 18 for a high-altitude point on the flight trajectory. This plot depicts the Mach 8 Tunnel B data and the Mach number, real gas, and viscous effects derived from CFD computations, finally arriving at the basic body C_m for flight conditions. Also shown in this figure are the preflight predictions of C_m for similar conditions. Note that the basic

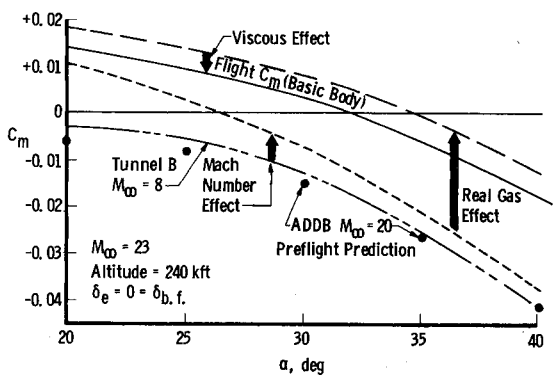

Fig. 18 Buildup of flight C_m using methodology model.

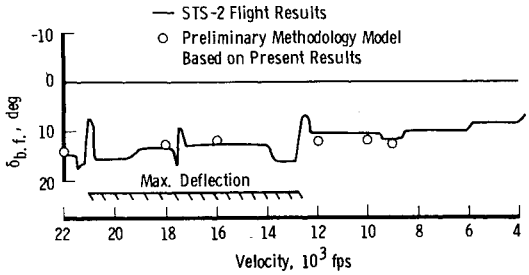

Fig. 19 Comparison of present results for body flap deflection with flight data.

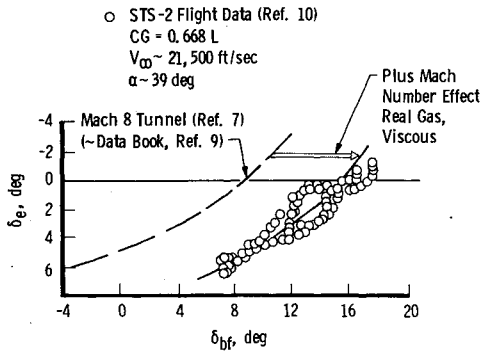

Fig. 20 Comparison of present results for body flap sweep with flight data.

body values of C_m based on the present results are over 0.02 greater than the preflight predictions.

Of particular interest in the comparisons with flight data are the body flap deflections required to maintain trim during re-entry. In the present analysis these were computed by selecting a velocity, altitude, angle of attack, and elevon deflection from flight data and iterating on the body flap deflection to make summation of moments on the vehicle equal to zero using the methodology shown in Fig. 17. The results of this calculation and comparison with STS-2 flight data are presented in Fig. 19. The present results are within 2 deg of the flight data over the entire high Mach number portion of the trajectory.

The body flap sweep at $M_\infty = 21$, where the body flap and elevons were deflected simultaneously to maintain the Orbiter in trim, was investigated in some detail. Displayed in Fig. 20 is the elevon deflection as a function of body flap angle obtained by using the $M_\infty = 8$ basic body pitching moment data. This dashed curve is very close to the preflight prediction. In addition, Fig. 20 shows the relationship between body flap deflection and elevon deflection during this sweep as computed by the present methodology and the corresponding flight data. The agreement is excellent.

Summary and Conclusions

Advanced CFD codes have been applied to a modified Orbiter geometry to obtain inviscid flowfield solutions for both wind tunnel and hypersonic flight conditions. A methodology model has been developed to extrapolate wind tunnel data to flight conditions. Computational results from the present study indicate that the differences between flight and pre-STS-1 predictions of hypersonic pitching moment are attributable primarily to Mach number and real gas effects.

Acknowledgments

This study was sponsored by the U.S. Air Force Space Division and Arnold Engineering Development Center. The authors wish to express appreciation to W.R. Martindale of Sverdrup Technology, Inc., for his advice and assistance in carrying out the computations and to Fred Shope of Calspan Field Services for his technical assistance throughout the study. Appreciation is also expressed to Harris Hamilton of NASA LaRC for the development of the model geometry used in this study.

The work reported herein was performed by the Arnold Engineering Development Center, Air Force Systems Command. The work and analysis was done by personnel of Calspan Field Services, Inc./AEDC Division, operating contractor for Aerospace Flight Dynamics Testing at AEDC. Further reproduction is authorized to satisfy needs of the U.S. Government.

References

[1] Young, J.C., Perez, L.F., Romere, P.O. and Kanipe, D.B., "Space Shuttle Entry Aerodynamic Comparisons of Flight 1 with Preflight Predictions," AIAA Paper 81-2476, Nov. 1981.

[2] Underwood, J.M. and Cooke, D.R., "A Preliminary Correlation of the Orbiter Stability and Control Aerodynamics from the First Two Space Shuttle Flights (STS-1 & 2) with Preflight Predictions," AIAA Paper 81-0564, March 1982.

[3] Hall, D.W., "Inviscid Aerodynamic Predictions for Ballistic Reentry Vehicles with Ablated Nosetips," SAI-79-506-VF, Science Applications, Inc., Valley Forge, Pa., Feb. 1979.

[4] Marconi, F., Salas, M., and Yaeger, L.S., "Development of a Computer Code for Calculating the Steady Super/Hypersonic Inviscid Flow Around Real Configurations," NASA CR-2675, April 1976.

[5] Vachris, A.F. and Yaeger, L.S., "Quick Geometry—A Rapid Response Method for Mathematically Modeling Configuration Geometry," NASA SP 390, 1975.

[6] Martindale, W.R. and Carter, L.D., "Flow Field Measurements in the Windward Surface Shock Layer of Space Shuttle Orbiter Configuration at Mach Number 8," AEDC-TR-75-5, July 1975.

[7] Jordan, J.L., "NASA/RI OA 208 and 209 Verification Static-Stability and Control-Effectiveness Tests of the Space Shuttle Orbiter Vehicle at Mach Numbers from 2 to 8," AEDC-TSR-78-V6, June 1978.

[8] Szema, K.Y., Griffith, B.J., Maus, J.R. and Best, J.T., "Viscous Flow Field Predictions on Shuttle-Like Vehicle Aerodynamics," AIAA Paper 83-0211, Jan. 1983.

[9] Russell, W.R., ed., "Aerodynamic Design Data Book, Volume 1, Orbiter Vehicle," Rockwell International, SD72-SD-0060, Oct. 1978.

[10] Office of Advanced Manned Vehicles, "Evaluation of the Space Shuttle Orbiter Second Orbital Flight—Descent Phase," Air Force Flight Test Center, Edwards Air Force Base, Calif., AFFTC-TR-82-1, Feb. 1982.